Weak anchoring effects in electrically driven Freedericksz transitions

2006 J. Phys. A: Math. Gen. 39 11

(http://iopscience.iop.org/0305-4470/39/1/002)

INSTITUTE OF PHYSICS PUBLISHING JOURNAL OF PHYSICS A: MATHEMATICAL AND GENERAL

J. Phys. A: Math. Gen. **39** (2006) 11–31 doi:10.1088/0305-4470/39/1/002

Weak anchoring effects in electrically driven Freedericksz transitions

Gaetano Napoli

Dipartimento di Matematica, Politecnico di Milano, Piazza Leonardo da Vinci 32-20133 Milano, Italy

Received 27 June 2005, in final form 29 September 2005
Published 7 December 2005
Online at stacks.iop.org/JPhysA/39/11

Abstract

We study the equilibrium configurations of a nematic liquid crystal confined between two parallel plates, when an electric field is applied. We take into account the mutual interaction of the field and the material. We also analyse the effects of two possibly different weak anchoring potentials at the plates. We use asymptotic methods to study in detail two different regimes of the applied voltage. The former concerns applied voltages close to the Freedericksz and the saturation critical thresholds; the latter is the case of high applied potentials. We discuss the new effects that arise with respect to the partial electric coupling and the strong anchoring cases.

PACS numbers: 61.30.−v, 61.30.Hn, 64.70.Md
Mathematics Subject Classification: 76A15, 82B27, 82B26

1. Introduction

A nematic liquid crystal [1] is a system of rod-like molecules whose mass centres do not exhibit any positional order. The interaction between neighbouring molecules tries to make them parallel to one another, and induces a partial ordering at mesoscopic scales. This effect competes against the distortions induced by external mechanical actions, electric or magnetic fields and the disordering thermal effects.

The classical elastic continuum theory is based on the pioneering works of Oseen [2], Zocher [3] and Frank [4]. A rigorous mathematical description of this theory can be found in [5]. The average alignment of the molecules is represented by a unit vector $\mathbf{n}$, called the director, where $\mathbf{n}$ is physically equivalent to $-\mathbf{n}$. In Frank's theory, a local stored energy function depending on $\mathbf{n}$ and its gradient is assumed. The director $\mathbf{n}$ adjusts throughout the sample in order to minimize that energy according to the boundary conditions.

Surface effects of liquid crystals are important for both device applications and basic understanding of physical phenomena [6]. The optical properties of devices containing nematic liquid crystals can be modified by altering the director field. In usual electro-optic devices the liquid crystal is confined between two parallel plates and its molecular orientation can be

driven through suitable actions at the boundaries. In practice it is possible to fix the molecules of liquid crystals at the boundary; delimiting surfaces can be treated in such a way that leads to a specific orientation of the molecules at the boundary. In some mathematical problems, the energy needed to destroy this anchoring, known as the *energy anchoring*, is assumed to be infinity. This assumption is called *strong anchoring* and consists in fixing *a priori* the value of **n** on the boundary. The boundary condition where the molecules are orthogonal to the delimiting surfaces is called *homeotropic*; on the other hand, when the optical axes are forced to be parallel to the boundary the condition is called *planar*. In some cases the effect of external actions succeeds in breaking the anchoring and the strong anchoring is not a correct assumption.

Rapini and Papoular [7] introduced first the *weak anchoring*. They proposed a formula for the anchoring energy. So, in the absence of external actions, the preferred direction of the molecules on the boundary minimizes the anchoring energy. The preferred direction is called the *easy axis*. In the presence of external actions, the direction of the molecules on the boundary is an unknown problem. Rapini–Papoular's formula has been confirmed in the experiment of Naermura [8].

The optical response of a cell containing a liquid crystal may be electrically driven by applying a voltage difference between the delimiting plates. In the presence of an electrostatic field the liquid crystal, considered as a perfect insulator, tends to align its molecules along or normal to the direction of the field, depending on the dielectric properties of the molecules. So, when a nematic liquid crystal is subject to an electric field, the free energy functional acquires a term which expresses the energy of interaction with the applied field. In addition, the distortion of the nematic director may affect the local electric field, so that the electric field itself obeys an equation fully coupled with the director equilibrium equation.

We consider a nematic liquid crystal sample which is initially in a planar homogeneous alignment. As it is discovered by Freedericksz [9], and well reported in [1, 5], at a critical value of the strength of the applied magnetic or electric field, a static distortion occurs. This phenomenon is called the Freedericksz transition and occurs with either strong or weak anchoring boundary conditions [5]. The post-critical response of simple cells containing nematic liquid crystals with strong anchoring boundary condition has been widely investigated in the literature [10–14].

The Freedericksz transition induced in samples of nematic with weak anchoring at the boundary, briefly called the *weak Freedericksz transition*, has been approached in [15] and analysed in detail, in the case of planar deformations, in [5]. The weak Freedericksz transition is similar to the classical one, until the external field becomes so strong that the preferred configuration becomes homogeneously homeotropic. When one considers an applied magnetic field, rather than an electric one, the field is not affected by nematic distortions. By analogy, we can consider the limit where the applied electric field is uncoupled from the other variables. We will refer to this assumption as the *magnetic approximation* [14].

In the present study we focus our attention on the non-trivial solutions of electrically driven Freedericksz transition cells. We investigate the effects due to the presence of a finite anchoring energy together with the complete electromechanical coupling. Our results generalize those obtained in [14] for strong anchoring to the case of weak anchoring and those reported in section 5.6 of [5] for partial field-matter coupling to the fully coupled case. We carried out some peculiar results for this specific problem. If we consider strong applied electric fields, we show that the anchoring strengths must scale in a suitable manner in order to avoid a homogeneous alignment of the molecules in the field direction. Whenever we assume different finite anchoring energies on the boundaries, we deduce that both the transition thresholds are decreasing monotonic functions of difference between the anchoring strengths.

This work is organized as follows. In section 2, we derive the governing equations for the specific problem considered in the rest of the paper: the plane deformation induced by an electrostatic field in a cell of nematic sandwiched between two parallel infinite plates. In sections 3 and 4, we assume equal anchoring energies at both plates, and we study the solution in two limiting cases: applied fields close to the Freedericksz and the saturation thresholds (section 3) and strong applied electric fields (section 4). In both these limits, we determine the director field and the electrostatic potential throughout the sample, with the aid of asymptotic methods. In section 5 we extend the results obtained in sections 3 and 4 by allowing the anchoring energies at the boundaries to be different. Some conclusions are pointed out in section 6.

2. Equilibrium equations

We consider a nematic liquid crystal confined between two parallel plates placed at $Z = -d/2$ and $Z = d/2$, subject to weak anchoring at the external surfaces. The easy axis is assumed to lie in the boundary planes, and will be labelled as X-axis. So, in the absence of any external action, the nematic is in homogeneous planar alignment. An electrical potential V_{app} is applied giving rise to an electrostatic field inside the nematic.

We assume plane deformations of the director field. In that case, the following representation of the director is possible $\mathbf{n} = (\cos\theta, 0, \sin\theta)$. The angle θ is determined by the director $\mathbf{n}$ and the X-axis and will be a function of Z coordinate only. Within these hypotheses, the Frank distortion energy per area unit [1, 4, 5] takes the form

$$W_F = \frac{1}{2}\int_{-d/2}^{d/2} (k_1 \cos^2\theta + k_3 \sin^2\theta)\left(\frac{\mathrm{d}\theta}{\mathrm{d}Z}\right)^2 \mathrm{d}Z. \tag{1}$$

In (1), k_1 and k_3 are two positive constants called the splay and the bend moduli, respectively. The contributions due to the twist and saddle-splay distortions vanish in our geometry (see, for example, [5]).

According to [1, 10], the interaction director field is described by the energy

$$W_I = -\frac{1}{2}\int_{-d/2}^{d/2} \mathbf{D}\cdot\mathbf{E}\,\mathrm{d}Z, \tag{2}$$

where $\mathbf{D} = \varepsilon_\perp \mathbf{E} + \varepsilon_a(\mathbf{E}\cdot\mathbf{n})\mathbf{n}$ is the dielectric displacement. The parameters $\varepsilon_\parallel$ and $\varepsilon_\perp$ are the static dielectric constant measured along or normal to the molecular axis, respectively; the quantity $\varepsilon_a = \varepsilon_\parallel - \varepsilon_\perp$ measures the dielectric anisotropy. By introducing the electrostatic potential Ψ, which also depends on the Z-coordinate only, we obtain

$$W_I = -\frac{1}{2}\int_{-d/2}^{d/2} (\varepsilon_\perp + \varepsilon_a \sin^2\theta)\left(\frac{\mathrm{d}\Psi}{\mathrm{d}Z}\right)^2 \mathrm{d}Z. \tag{3}$$

It is easy to check that, whenever ε_a is positive, the molecules prefer to align their axes along the electric field direction. For any future development we assume $\varepsilon_a > 0$ in order to create competition between the electric field and the surface anchoring.

The anchoring at the boundaries is described by the Rapini–Papoular energy:

$$W_A = \frac{w^\pm}{2}\sin^2\theta \qquad \text{at} \qquad Z = \pm\frac{d}{2}, \tag{4}$$

where both anchoring strengths w^+ and w^- are positive. With this choice of $w^\pm$, the anchoring energy is minimized when $\mathbf{n}$ is parallel to the plates. It favours the planar easy axes.

The total energy per area unit is then

$$W = W_F + W_I + W_A. \tag{5}$$

In order to obtain the Euler–Lagrange equations, we vary the total energy W. The first variation of W is defined as

$$\delta W = \left[\frac{\partial}{\partial\lambda} W(\theta + \lambda\delta\theta, \theta' + \lambda\delta\theta', \Psi' + \lambda\delta\Psi')\right]_{\lambda=0}, \tag{6}$$

where $(\cdot)'$ denotes the derivative with respect to Z. By using (6) and applying the divergence theorem we obtain

$$\begin{aligned}\delta W = -\int_{-d/2}^{d/2} \Bigg\{ \Bigg[& 2(k_1\cos^2\theta + k_3\sin^2\theta)\frac{\mathrm{d}^2\theta}{\mathrm{d}Z^2} + (k_3 - k_1)\sin 2\theta\left(\frac{\mathrm{d}\theta}{\mathrm{d}Z}\right)^2 \\ & + \varepsilon_a \sin 2\theta\left(\frac{\mathrm{d}\Psi}{\mathrm{d}Z}\right)^2\Bigg]\delta\theta - \frac{\mathrm{d}}{\mathrm{d}Z}\left[(\varepsilon_\parallel \sin^2\theta + \varepsilon_\perp\cos^2\theta)\frac{\mathrm{d}\Psi}{\mathrm{d}Z}\right]\delta\Psi\Bigg\}\,\mathrm{d}Z \\ & + \left\{\left[2(k_1\cos^2\theta + k_3\sin^2\theta)\frac{\mathrm{d}\theta}{\mathrm{d}Z} + w^+\sin 2\theta\right]\delta\theta\right\}_{Z=d/2} \\ & + \left\{\left[-2(k_1\cos^2\theta + k_3\sin^2\theta)\frac{\mathrm{d}\theta}{\mathrm{d}Z} + w^-\sin 2\theta\right]\delta\theta\right\}_{Z=-d/2}.\end{aligned} \tag{7}$$

Note that $\delta\Psi$ vanishes on the boundary since the potential is imposed on it.

At the equilibrium $\delta W = 0$. Taking into account the arbitrariness of $\delta\theta$ and $\delta\Psi$ we obtain the bulk equilibrium equations

$$2(k_1\cos^2\theta + k_3\sin^2\theta)\frac{\mathrm{d}^2\theta}{\mathrm{d}Z^2} + (k_3 - k_1)\sin 2\theta\left(\frac{\mathrm{d}\theta}{\mathrm{d}Z}\right)^2 + \varepsilon_a\sin 2\theta\left(\frac{\mathrm{d}\Psi}{\mathrm{d}Z}\right)^2 = 0, \tag{8}$$

and

$$\frac{\mathrm{d}}{\mathrm{d}Z}\left[(\varepsilon_\parallel\sin^2\theta + \varepsilon_\perp\cos^2\theta)\frac{\mathrm{d}\Psi}{\mathrm{d}Z}\right] = 0, \tag{9}$$

and the boundary conditions

$$2(k_1\cos^2\theta + k_3\sin^2\theta)\frac{\mathrm{d}\theta}{\mathrm{d}Z} \pm w^\pm\sin 2\theta = 0, \qquad \text{at} \quad Z = \pm\frac{d}{2}, \tag{10}$$

and

$$\Psi = \pm\frac{V_{\mathrm{app}}}{2} \qquad \text{at} \qquad Z = \pm\frac{d}{2}. \tag{11}$$

As is to be expected, the bulk equations (8) and (9) are identical to equations (3.1) and (3.2) of [14]. Also the electrical boundary conditions (11) are unchanged. Nevertheless, the introduction of the anchoring energy W_A modifies the boundary conditions on the director (compare equation (10) with equation $(3.3)_I$ in [14]). In fact, on the boundaries the director $\mathbf{n}$ will adjust itself in order to satisfy (10), while the case planar strong anchoring, analysed in [14], fixes *a priori* its value to be zero.

2.1. Dimensionless equations

To better discuss our results, we now write the equilibrium equations in dimensionless form. We introduce the scaled variables

$$z = \frac{Z}{d}, \qquad \psi = \frac{\Psi}{V_{\mathrm{app}}}, \tag{12}$$

and define the dimensionless scalars

$$\alpha = \frac{k_3}{k_1} - 1, \qquad \eta = 1 - \frac{\varepsilon_\perp}{\varepsilon_\parallel}, \qquad V = \sqrt{\frac{\varepsilon_a}{k_1}}V_{\mathrm{app}}, \qquad \beta^\pm = \frac{\mathrm{d}w^\pm}{k_1}, \tag{13}$$

which represent the dimensionless nematic anisotropy, dielectric anisotropy, applied voltage and anchoring strengths, respectively. The quantity $\xi = k_1/w$, called the *extrapolation length*, is the measure for the relevance of the competing elastic distortion versus the anchoring-induced order. The ratio between the sample thickness d and the extrapolation length measures the robustness of the anchoring. We may recover the strong planar anchoring by performing the $\beta^{\pm} \to \infty$ limit in equation (10), while free boundary conditions are obtained in the $\beta^{\pm} \to 0$ limit.

Our problem is now restricted to the interval $z \in [-1/2, 1/2]$. We introduce the following notation: plus and/or minus superscripts denote function values in $z = 1/2$ and/or $z = -1/2$, respectively. The bulk equations (8) and (9) now become

$$2(1 + \alpha \sin^2\theta)\theta_{zz} + \alpha \sin 2\theta\theta_z^2 + \sin 2\theta V^2\psi_z^2 = 0, \tag{14}$$

and

$$[(1 - \eta \cos^2\theta)\psi_z]_z = 0. \tag{15}$$

The boundary conditions (10) and (11) read

$$2(1 + \alpha \sin^2\theta^{\pm})\theta_z^{\pm} \pm \beta^{\pm} \sin 2\theta^{\pm} = 0, \qquad \text{and} \qquad \psi^{\pm} = \pm 1/2. \tag{16}$$

Self *et al* [14] first performed a systematic study of the solutions of (14)–(16) considering strong planar anchoring boundary conditions. They take into account the various physically relevant distinguished limiting cases of the parameters α, η and V, and derived approximate solutions using asymptotic methods. In the low-field and small dielectric anisotropy regime they recovered the results of [10] and [12]. In the high-field they approached the solution through boundary layer methods. The excellent agreement of the so-obtained solutions with the numerical ones shows the usefulness of the adopted methods. We perform a similar analysis to understand the effect of weak anchoring in the same limiting cases. Nevertheless, a first difference between our problem and that analysed in [14] arises from the presence of two further additional parameters, the dimensionless anchoring strengths $\beta^{\pm}$. Since we have assumed $w^{\pm}$ to be positive, we have $\beta^{\pm} \in [0, \infty)$. The delimiting values of this range correspond to free and strong planar anchoring boundary conditions, respectively.

The dimensionless equilibrium equations (14) and (15), together with the boundary conditions (16), admit the trivial solutions

$$\{\theta = 0, \psi = z\}, \qquad \{\theta = \pi/2, \psi = z\}. \tag{17}$$

Note that in the presence of strong planar anchoring boundary conditions, the second solution must be discarded since it does not satisfy the boundary conditions. In addition, the existence of the two trivial solutions (17) yields the existence of two critical bifurcation values, rather than the only one that can be found in the strong anchoring limit.

We first consider the case in which the anchoring strengths on both plates are equal: $\beta^+ = \beta^- = \beta$. We will treat the case of different anchoring strengths in section 5. Close to the Freedericksz transitions, the results derived in section 5.6 of [5] still hold. There are two critical values of V, namely V_F and V_S, such that for any $V \in (V_F, V_S)$ the equilibrium equations admit non-trivial solutions with lower energy than the trivial ones. These critical values obey the equations

$$\frac{V_F}{\beta} = \cot\frac{V_F}{2}, \tag{18}$$

and

$$\sqrt{1+\alpha}\,\frac{V_S}{\beta} = \coth\left(\frac{V_S}{2\sqrt{1+\alpha}}\right), \tag{19}$$

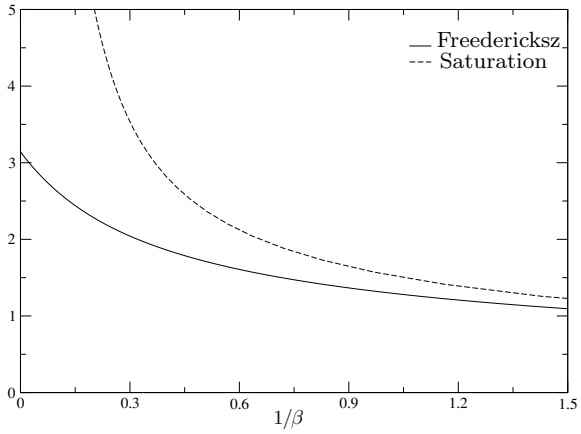

Figure 1. Plots of the transition critical thresholds as functions of inverse of the anchoring strength.

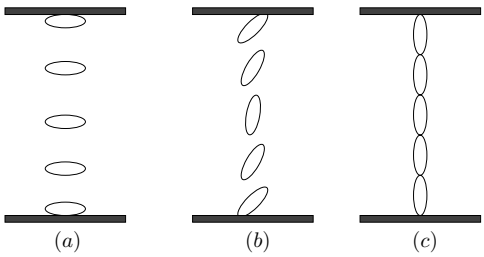

Figure 2. Schematic representation of weak Freedericksz transition: *(a)* homogeneous planar alignment; *(b)* distorted configuration; *(c)* homogeneous homeotropic alignment.

respectively. Note that $V_F \leqslant V_S$ for all β. In the limit of infinitely strong anchoring energies, V_F tends to π, in agreement with the classical Freedericksz threshold, and V_S tends to infinity. For very weak anchoring energies, both V_F and V_S tend to zero. We will refer to V_F and V_S as the Freedericksz and the saturation thresholds, respectively. Figure 1 shows the plot of the Freedericksz thresholds as functions of the inverse of the dimensionless anchoring strength.

Let us now see what is the physical meaning of V_F and V_S. When a potential difference is established between the plates, the nematic molecules initially in a planar homogeneous configuration (figure 2(a)) tend to rotate their axes towards the Z direction. On the other hand, the molecules prefer to maintain their axes parallel to one another and, possibly, in the direction of the easy axis. At $V_F < V < V_S$ the electric torque prevails on the nematic actions. Nevertheless, the anchoring strength is strong enough to recall the director of the molecules at the boundary, in the direction of the easy axes. The compromise is a non-homogeneous configuration of the director field where $|\theta|$ reaches its maximum values in the middle of the cell and the minimum on the boundary (figure 2(b)). At $V > V_S$ the electric torque is strong enough to destroy the anchoring. Then the molecules prefer to orient themselves parallel to each other in the direction of the field, in a homogeneous homeotropic texture (figure 2(c)). In the case of strong anchoring the electric energy required to destroy the anchoring is infinite and therefore V_S diverges in the limit $\beta \to \infty$. By contrast, when $\beta \to 0$ the molecules at the boundary are freely orientable and an infinitesimal electric field is able to reorient the molecules through the sample in a homogeneous homeotropic alignment. Thus, both thresholds become infinitesimal and the distorted zone vanishes.

Note that, taking into account the β definition and equations (18) and (19), it follows by that keeping unaltered the constitutive parameters of the nematic and the anchoring strengths, the critical thresholds increase with the sample thickness. Therefore, in very thin cells the Freedericksz and the saturation transitions are achieved for very low applied voltages.

3. Solutions close to the critical voltages

In this section we determine the shape of the solutions of the equilibrium equations close to the bifurcation points. Here the difficulty arising from the complete electromechanical coupling combines with the difficulties arising from the implicit equations (18) and (19). However, the deduced results can both be compared with the numerical results and analysed in special cases, where one recovers the already known results.

3.1. Applied voltages just above V_F

Let us consider a reduced applied voltage V slightly higher than V_F:

$$V = V_F(1 + \delta^2), \qquad \delta \ll 1. \tag{20}$$

Consistently, we assume that the unknown fields are slightly perturbed with respect to the trivial solution $\{\theta = 0, \psi = z\}$

$$\theta(z) = \delta\theta_1(z) + \delta^2\theta_2(z) + \delta^3\theta_3(z) + o(\delta^3) \tag{21}$$

$$\psi(z) = z + \delta\psi_1(z) + \delta^2\psi_2(z) + \delta^3\psi_3(z) + o(\delta^3). \tag{22}$$

By replacing (21) and (22) into (14)–(16), we obtain at $O(\delta)$ the dimensionless linearized bulk equilibrium equations

$$\theta_{1zz} + V^2\theta_1 = 0, \qquad \psi_{1zz} = 0, \tag{23}$$

and the dimensionless linearized boundary conditions

$$\theta_{1z}^{\pm} \pm \beta\theta_1^{\pm} = 0, \qquad \psi_1^{\pm} = 0. \tag{24}$$

By solving the linearized equations, one finds an infinity of solutions: one with homogeneous planar alignment, which corresponds to the solution $\theta_1 = 0$ and a double infinity with distorted nematic director where

$$\theta_1 = A\cos(V_F z), \tag{25}$$

with V_F satisfying equation (18). In fact, from the periodicity of the trigonometric functions, equation (18) admits a double infinity of solutions for any fixed β. These solutions are symmetrical with respect to $V_F = 0$, since positive and negative applied voltages lead to the same distorted configuration.

By pushing to higher orders the perturbation algorithm we find

$$\theta(z) = \delta A\cos(V_F z) + o(\delta^2), \tag{26}$$

$$\psi(z) = z + \delta^2\left[-\frac{A^2\eta}{\varpi}\sin(2V_F z) + Bz\right] + o(\delta^2). \tag{27}$$

As is to be expected, θ and ψ are respectively an even and an odd function in $z \in [-1/2, 1/2]$. The determination of the constants A and B involves the first nonlinearity of the problem,

which occurs at $O(\delta^3)$. So, the equation for θ_3 is

$$\theta_{3zz} + V_F^2\theta_3 = A^3 V_F^2 \cos(V_F z)\left[\left(\alpha + \frac{\eta}{1-\eta}\right)\cos(2V_F z) + \frac{2}{3}\cos^2(V_F z) + \frac{2\eta\beta}{(\eta-1)\left(V_F^2+\beta^2\right)}\right], \tag{28}$$

which admits the general solution

$$\theta_3 = A_3\cos(V_F z) + C_3\sin(V_F z) + \frac{A^3}{8(\eta-1)\left(V_F^2+\beta^2\right)}\left[-\frac{1}{2}\left((\eta-1)\alpha - \frac{2}{3}\eta - \frac{1}{2}\right)\times\left(V_F^2+\beta^2\right)\cos(3V_F z) + (\cos(V_F z) + 2\sin(V_F z)V_F z)\left(\varpi V_F^2 + (\varpi\beta + 4\eta)\beta\right)\right], \tag{29}$$

where $\varpi = 1 + \alpha(1-\eta)$ and β and V_F are related through equation (18).

By substituting (21) into (16) and retaining just the $O(\delta^3)$ terms, we obtain the boundary conditions

$$\theta_{3z}^{\pm} \pm \beta\theta_3^{\pm} = \pm A^3\cos^2\frac{V_F}{2}\left[\alpha V_F \sin\frac{V_F}{2} + \frac{2}{3}\beta\cos\frac{V_F}{2}\right]. \tag{30}$$

By replacing (30) into (29) we find the first-order amplitude expression

$$A = \pm 2\sqrt{\frac{(1-\eta)\left(V_F^2+\beta^2\right)\left(V_F^2+2\beta+\beta^2\right)}{\left(\beta^4+2\beta^3+2\beta^2V_F^2-2\beta V_F^2+V_F^4\right)\varpi + 4\eta\beta\left(V_F^2-\beta^2-2\beta\right)}} \tag{31}$$

and consequently

$$B = \frac{\eta\beta A^2}{(1-\eta)\left(V_F^2+\beta^2\right)}. \tag{32}$$

In our approximation δA represents the value of $\theta(z)$ in the middle of the cell, which could be positive or negative depending on whether the molecules rotate in anticlockwise or clockwise direction, respectively.

The numerical counterpart of the problem is performed as follows. For all given δ and β, we solve the complete nonlinear problem assuming an adimensional applied voltage $V = V_F(1+\delta^2)$. V_F is obtained by solving numerically equation (18). To estimate the difference between the numerical and the approximate solutions we define their relative mismatch

$$\mathrm{Err} = \frac{\int_{-1/2}^{1/2}|\theta_{\mathrm{appr}} - \theta_{\mathrm{num}}|^2\,\mathrm{d}z}{\int_{-1/2}^{1/2}|\theta_{\mathrm{num}}|^2\,\mathrm{d}z}. \tag{33}$$

Figure 3 (left) shows the plot of Err as a function of δ for different values of β. The difference between the numerical and approximate solutions tends to zero with δ.

For high but not infinite anchoring strength, (31) and (32) become

$$A = \pm 2\sqrt{\frac{1-\eta}{\varpi}}\left(1 + \frac{2\eta}{\varpi\beta}\right) + O\left(\frac{1}{\beta^2}\right), \tag{34}$$

$$B = \frac{4\eta}{\varpi\beta} + O\left(\frac{1}{\beta^2}\right). \tag{35}$$

Note that the factor under square root in (34) is always positive. In fact, $\eta \in (0, 1]$ since $\epsilon_a > 0$. On the other hand, $\alpha \geqslant -1$ by definition and, therefore, ϖ is positive.

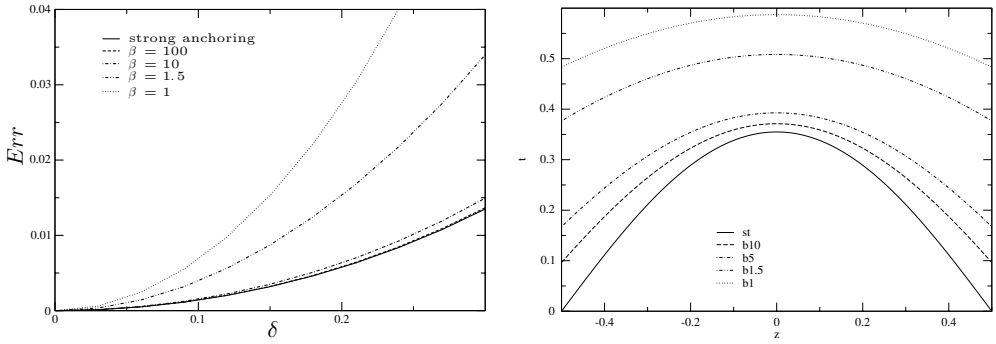

Figure 3. Left: plot of the relative mismatch between the numerical and the approximate solutions close to the Freedericksz transition, for several values of dimensionless anchoring strength β. The function Err tends to zero with δ and therefore the approximate solution tends to the numerical one for infinitesimal δ. Right: plots of θ profile close to the Freedericksz threshold, for several values of β and $\delta = 0.2$. The curve $\theta(z)$ moves upwards as β decreases and therefore θ^+ and A are decreasing functions of β. Both plots are obtained by setting $\eta = 0.2$ and $\alpha = 0$.

3.2. Applied voltages just below V_S

For a given β, a critical voltage V_S given by (19) exists below which non-trivial solutions are possible. Let us suppose now that the applied voltage can be written as

$$V = V_S(1 - \delta^2), \tag{36}$$

where δ is infinitesimal. Consequently, we assume slight perturbed solutions with respect to the trivial solution $\{\theta = \pi/2, \psi = z\}$:

$$\theta(z) = \pi/2 + \delta\bar{\theta}_1(z) + \delta^2\bar{\theta}_2(z) + \delta^3\bar{\theta}_3(z) + o(\delta^3), \tag{37}$$

$$\psi(z) = z + \delta\bar{\psi}_1(z) + \delta^2\bar{\psi}_2(z) + \delta^2\bar{\psi}_3(z) + o(\delta^3). \tag{38}$$

By inserting (37) and (38) into (14)–(16) and retaining just the $O(\delta)$ terms, we arrive at the linear equilibrium equations and boundary conditions:

$$\iota\bar{\theta}_{1zz} - V^2\bar{\theta}_1 = 0, \qquad \bar{\psi}_{1zz} = 0, \tag{39}$$

$$\iota\bar{\theta}_{1z}^{\pm} \mp \beta\bar{\theta}_1^{\pm} = 0, \qquad \bar{\psi}_1^{\pm} = 0, \tag{40}$$

where $\iota = 1 + \alpha$. Equation $(39)_1$ together with the boundary condition $(40)_1$ gives a double infinity of solutions. The trivial solution $\bar{\theta}_1 = 0$ corresponds to the homogeneously homeotropic configuration. The non-trivial solutions are of the form

$$\bar{\theta}_1 = \bar{A}\cosh\left(\frac{V_S z}{\sqrt{\iota}}\right), \tag{41}$$

where V_S is given through (19). In addition, for all fixed β the lowest (in modulus) root V_S of equation (19) determines the saturation threshold.

As before, the linearized problem is partially coupled. The correction of the electrostatic potential occurs at $O(\delta^2)$ and the determination of $\bar{A}$ requires the $\bar{\theta}_3$ equilibrium equation. According to standard techniques of perturbation theory, we push our algorithm up to $O(\delta^3)$

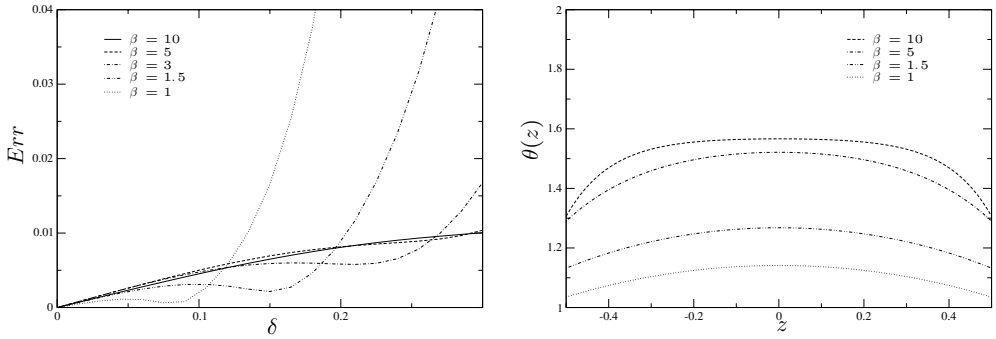

Figure 4. Left: plot of the relative mismatch between the numerical and the approximate solutions close to the saturation transition, for different values of dimensionless anchoring strength β. Err(δ) tends to zero with δ and therefore the approximate solution tends to the numerical one for infinitesimal δ. Right: plots of θ profile near the saturation threshold, for several β and $\delta = 0.2$. The curves $\theta(z)$ move downwards as the value of β decreases and therefore θ^+ and $\bar{A}$ are an increasing and a decreasing function of β, respectively. Both plots are obtained by setting $\eta = 0.2$ and $\alpha = 0$.

obtaining

$$\theta(z) = \frac{\pi}{2} + \delta \bar{A} \cosh\left(\frac{V_S z}{\sqrt{\iota}}\right) + o(\delta^2), \tag{42}$$

$$\psi(z) = z + \delta^2 \left[-\frac{\bar{A}^2 \eta \sqrt{\iota}}{4\varpi V_S} \sinh\left(\frac{2V_S z}{\sqrt{\iota}}\right) + \bar{B} z \right] + o(\delta^2), \tag{43}$$

with

$$\bar{A} = \pm 2 \sqrt{\frac{\iota\left(\iota V_S^2 + 2\iota\beta - \beta^2\right)\left(\beta^2 - \iota V_S^2\right)}{\left(\beta^4 + \iota^2 V_S^4\right)(\iota\eta + 1) + 2\beta\iota\left(\beta^2 + \iota V_S^2\right)(\iota\eta - 1) - 2\iota\beta^2\left(\iota\eta V_S^2 + 4\iota^2\eta + V_S^2\right)}}, \tag{44}$$

and

$$\bar{B} = \frac{\eta\beta\iota\bar{A}^2}{V_S^2\iota - \beta^2}, \tag{45}$$

where β can be expressed as a function of V_S through (19). By equation (44) it follows that θ can assume equivalently values slightly less or higher than $\pi/2$.

As figure 4 shows, the approximate solution tends to the numerical one for infinitesimal δ.

3.3. Discussion

The analysis performed in the two previous subsections yields the solution of our problem in a neighbourhood of the Freedericksz critical fields. Our analysis goes beyond the linear approximation allowing us to determine completely the main order correction to each trivial solution. By contrast, the results reported in section 5.6 of [5] are limited to the linear analysis and, therefore, give just the form of the $O(\delta)$ correction, without determination of its amplitude. In addition, the linear analysis alone is not able to establish the influence of the complete electromechanical coupling. In fact, the correction to the electric potential is $O(\delta^2)$ and the effect of the coupling is contained in the expressions of A and $\bar{A}$, which are determined at $O(\delta^3)$. The magnetic approximation can be obtained by setting $\eta = 0$. In this limit both B and $\bar{B}$ vanish, and therefore the correction to the electrostatic potential vanishes.

Deuling [10], Schiller [12] and Self *et al* [14] considered the fully coupled electromechanical problem with planar strong anchoring boundary conditions. In this case the only finite Freedericksz threshold is equal to π and, therefore, the search of solutions close to the bifurcation point becomes quite simplified with respect to ours. The values of A and B reduce to the first term only in the expressions (34) and (35), respectively. We have recovered the classical results (compare our results with equations (4.1) and (4.2) of [14]) in the limit $\beta \to \infty$.

As for the solution close to the saturation bifurcation, in the limit of high anchoring strength, it follows from (19) that $\beta \approx \sqrt{\iota} V_S$. Consequently, $\bar{A} = o(\beta^{-3/2})$ and $\bar{B} \approx -\sqrt{\iota}/\beta$. On the boundary $\theta^+ \approx \pi/2 \pm 2\delta\iota\beta^{-3/2}$. We stress the fact that at first we fix V_S, or equivalently β, and then we consider infinitesimal perturbation of the applied voltage. Only in this order of limits we can obtain a regular solution in a neighbourhood of the critical potential V_S. By contrast, if we fix δ and consider β tending to infinity, non-regular solutions are to be expected.

Finally, we observe (figure 3 left) that the convergence close to the Freedericksz transition is monotonic with β, while this feature is not verified close to the saturation transition (figure 4 left). However, the complete analytic behaviour of $\mathrm{Err}(\delta)$ can be determined by only pushing the solutions asymptotic development to higher orders.

4. High applied voltages

In this section, we consider the case where a high voltage is applied. In other words, we assume that the dimensionless applied voltage V is much larger than the other dimensionless parameters.

The case with strong planar anchoring boundary conditions and high applied voltages has been carefully analysed in [14]. The authors highlight three different regions for the θ profile. A thick one extends in most of the interior of the cell where θ changes smoothly. In two thin symmetrical regions adjacent to the plates, θ changes rapidly. This behaviour can be qualitatively explained as follows. Inside the cell and away from the plates, the anchoring effects are negligible. The electric torque prevails and the molecules align to the field direction. Though the applied voltage field is strong, V remains finite, while the anchoring strength is assumed to be infinity. Therefore, the molecules at the boundary are forced to remain parallel to the plates. In the thin regions θ should vary from 0 to $\pi/2$. Since the dimensionless applied potential is quite large, the gradient of θ becomes very large and, consequently, all terms in the director equation are of the same order of magnitude.

Our aim is to extend the above results to the case of weak anchoring boundary conditions. In this case the behaviour is very similar to the case of strong anchoring boundary conditions, provided that the reduced applied voltage remains under the saturation threshold V_S. Otherwise, the anchoring breaks and all molecules align their axes in the field direction. As in [14], we introduce the parameter $\epsilon = 1/V$, with $\epsilon \ll 1$. By equation (19), it follows that β must be rescaled as $\beta = \bar{\beta}/\epsilon^\gamma$, where $\bar{\beta}$ is $O(1)$ and $\gamma \geqslant 1$; otherwise we reach the trivial solution $\{\theta = \pi, \psi = z\}$. Note that the dimensionless anchoring strength is an increasing function of γ.

We limit our analysis to small dielectric anisotropies $\eta = \epsilon\bar{\eta}$, where $\bar{\eta}$ is $O(1)$, and *one constant approximation* $\alpha = 0$. The case of small nematic anisotropy will be discussed in subsection 4.4. In the hypothesis of small dielectric anisotropies, one constant approximation and high applied voltage, the bulk equilibrium equations take the form

$$2\epsilon^2\theta_{zz} + \sin 2\theta\,\psi_z^2 = 0, \tag{46}$$

$$[(1 - \epsilon\bar{\eta}\cos^2\theta)\psi_z]_z = 0, \tag{47}$$

while the boundary conditions become

$$2\epsilon^{\gamma}\theta_z^{\pm} \pm \bar{\beta}\sin 2\theta^{\pm} = 0, \tag{48}$$

$$\psi^{\pm} = \pm 1/2. \tag{49}$$

In the singular limit $\epsilon \to 0$ we expect a zone far from the boundaries where the solution changes smoothly and two narrow regions close to the boundaries where the solution changes rapidly. These thin regions are called *boundary layers* [16]. Usually one tries to obtain the solution by solving exactly a sequence of approximate problems. One starts by treating the problem as a regular perturbation by producing what is known as the *outer approximation*. The problem in the narrows regions, called the *inner approximation*, is studied by introducing suitable stretched coordinates. The inner and the outer expansions must overlap in an intermediate region. Forcing the two expansions to coincide in this region determines the coefficients of the expansions. This process is called *asymptotic matching*. As a final result one obtains a *composite solution* by adding the inner and the outer, and then subtracting their common expression in the overlap region. However, a detailed and exhaustive treatment of this technique can be found in [16].

4.1. Outer approximation

In this region $z = O(1)$ and the solution admits a regular expansion in ϵ:

$$\widehat{\theta} = \widehat{\theta}_0 + \sum_{i=1}^{\infty} \epsilon^i \widehat{\theta}_i, \qquad \widehat{\psi} = \widehat{\psi}_0 + \sum_{i=1}^{\infty} \epsilon^i \widehat{\psi}_i. \tag{50}$$

If we replace this expansion in equations (46) and (47), we find that any constant integer multiple of $\pi/2$ satisfies the outer equation. We focus our attention on the solution of the type

$$\widehat{\theta}_0 = \frac{\pi}{2}, \qquad \widehat{\theta}_i = 0 \quad i \geqslant 1, \tag{51}$$

$$\widehat{\psi}_i = a_i z + b_i, \qquad i \geqslant 0. \tag{52}$$

The other physically relevant solution is $\widehat{\theta}_0 = 0$, which does not produce boundary layers. The constants a_i, b_i will be determined by matching the inner and the outer approximations.

4.2. Inner approximations

Following [14], in order to make the second derivative term $O(1)$ we use the re-scaling $z = -1/2 + \epsilon\zeta$ in the left narrow region and $z = 1/2 - \epsilon\zeta$ in the right one. The so-rescaled bulk equilibrium equations are identical in both narrow regions, so we limit our analysis just to the left thin zone. The solution in the right one can be obtained by symmetry. By rescaling equations (46) and (47) we obtain

$$2\epsilon^2\widetilde{\theta}_{\zeta\zeta} + \sin 2\widetilde{\theta}\widetilde{\psi}_{\zeta}^2 = 0 \qquad \text{and} \qquad [(1 - \epsilon\bar{\eta}\cos^2\widetilde{\theta})\widetilde{\psi}_{\zeta}]_{\zeta} = 0, \tag{53}$$

where $\widetilde{\theta}$ and $\widetilde{\psi}$ are functions of the stretched variable ζ. The boundary conditions (48) and (49) become

$$2\epsilon^{\gamma-1}\widetilde{\theta}_{\zeta}^{-} - \bar{\beta}\sin 2\widetilde{\theta}^{-} = 0 \qquad \text{and} \qquad \widetilde{\psi}^{-} = -1/2, \tag{54}$$

where the minus superscript denotes now the value of the function at $\zeta = 0$. We expand $\widetilde{\theta}$ and $\widetilde{\psi}$ as

$$\widetilde{\theta} = \widetilde{\theta}_0 + \sum_{i=1}^{\infty} \epsilon^i \widetilde{\theta}_i \qquad \text{and} \qquad \widetilde{\psi} = \widetilde{\psi}_0 + \sum_{i=1}^{\infty} \epsilon^i \widetilde{\psi}_i. \tag{55}$$

If we insert (55) into $(53)_{II}$ and $(54)_{II}$, we obtain at $O(\epsilon)$ the solutions

$$\widetilde{\psi}_0 = A_0\zeta + B_0, \qquad \widetilde{\psi}_1 = A_1\zeta + B_1, \tag{56}$$

and the boundary conditions $\widetilde{\psi}_0^- = -1/2$ and $\widetilde{\psi}_1^- = 0$ which imply $B_0 = -\frac{1}{2}$, $B_1 = 0$. Also, the $O(1)$ matching of inner and outer solution gives $A_0 = 0$.

If we push the expansion to $O(\epsilon^2)$, equation $(53)_I$ gives

$$2\widetilde{\theta}_{0\zeta\zeta} + A_1^2 \sin 2\widetilde{\theta}_0 = 0; \tag{57}$$

the integration of this equation, taking into account the matching with the outer solution which implies $\widetilde{\theta}_0(\infty) = \pi/2$ and $\widetilde{\theta}_{0\zeta}(\infty) = 0^+$, gives

$$\widetilde{\theta}_0 = 2\arctan\frac{C_0\,\mathrm{e}^{A_1\zeta} - 1}{C_0\,\mathrm{e}^{A_1\zeta} + 1}, \tag{58}$$

where C_0 will be determined below with the aid of $(54)_I$. We remark that the matching condition $\widetilde{\theta}_0(\infty) = \pi/2$ with $\widetilde{\theta}_{0\zeta}(\infty) = 0^-$ is equally possible. The corresponding solution is the mirror-like one of (58) with respect to the ζ-axis. We also note that

$$C_0 = \frac{1 + \tan\frac{\widetilde{\theta}_0^-}{2}}{1 - \tan\frac{\widetilde{\theta}_0^-}{2}} \in [1, \infty). \tag{59}$$

The case $C_0 = 1$ corresponds to the strong anchoring boundary conditions, while in the limit $C_0 \to \infty$ the boundary layers vanish. Thus, the singular solution approaches a regular one by increasing C_0.

The $O(\epsilon^2)$ equation for $\widetilde{\psi}$ reads

$$\widetilde{\psi}_{2\zeta} = A_2 + \bar{\eta}A_1\cos^2\widetilde{\theta}_0. \tag{60}$$

If we substitute (58) into the latter equation, perform the integration and also impose $\widetilde{\psi}_2(0) = 0$, we obtain

$$\widetilde{\psi}_2(\zeta) = A_2\zeta + \frac{4\bar{\eta}C_0^2\tanh(A_1\zeta)}{\big(C_0^2+1\big)\big[\big(C_0^2-1\big)\tanh(A_1\zeta) + C_0^2 + 1\big]}. \tag{61}$$

In a similar way, we can obtain the right inner approximation. The asymptotic matching between inner and outer solutions determines all the coefficients involved in the expansions. Therefore, as inner solutions we obtain

$$\widetilde{\psi}^l(\zeta) \approx -\frac{1}{2} + \epsilon\zeta + \epsilon^2\frac{4\bar{\eta}C_0^2\tanh\zeta}{\big(C_0^2+1\big)\big[\big(C_0^2-1\big)\tanh\zeta + C_0^2 + 1\big]} \approx -\widetilde{\psi}^r(\zeta), \tag{62}$$

while for the outer expansion we have

$$\widehat{\psi} \approx z - \epsilon^2\frac{2\bar{\eta}}{C_0^2+1}z. \tag{63}$$

The equation for $\widetilde{\theta}_1$ is

$$\widetilde{\theta}_{1\zeta\zeta} + \widetilde{\theta}_1\cos 2\widetilde{\theta}_0 = 2\bar{\eta}\widetilde{\theta}_{0\zeta\zeta}\cos^2\widetilde{\theta}_0, \tag{64}$$

which, when integrated with the condition $\widetilde{\theta}_1(\infty) = 0$, leads to

$$\widetilde{\theta}_1(\zeta) = -\frac{2C_0\bar{\eta}\,\mathrm{e}^{\zeta}}{\big(C_0^2\,\mathrm{e}^{2\zeta}+1\big)^2} + \frac{C_1\,\mathrm{e}^{\zeta}}{C_0^2\,\mathrm{e}^{2\zeta}+1}. \tag{65}$$

The constant C_1 will be determined below by using the anchoring condition on $\widetilde{\theta}_1$. Finally the expression of $\widetilde{\theta}$ in the left and right narrow regions is

$$\widetilde{\theta}^l(\zeta) \approx 2\arctan\frac{C_0\,\mathrm{e}^{A_1\zeta}-1}{C_0\,\mathrm{e}^{A_1\zeta}+1} - \epsilon\frac{2C_0\bar{\eta}\,\mathrm{e}^{\zeta}}{\left(C_0^2\,\mathrm{e}^{2\zeta}+1\right)^2} + \epsilon\frac{C_1\,\mathrm{e}^{\zeta}}{C_0^2\,\mathrm{e}^{2\zeta}+1} \approx \widetilde{\theta}^r(\zeta). \quad (66)$$

4.3. Composite solution

The composite approximation of the equilibrium configuration is obtained by adding the inner and the outer, and then subtracting the common expression in the overlap regions. This rule when applied to (62), (63), (51) and (66) gives respectively the composite expressions

$$\psi^c(z) \approx z - \epsilon^2\frac{2\bar{\eta}}{C_0^2+1}z + \epsilon^2\frac{4\bar{\eta}C_0^2}{C_0^2+1}\left(\frac{\tanh\frac{1+2z}{2\epsilon}}{\left(C_0^2-1\right)\tanh\frac{1+2z}{2\epsilon}+C_0^2+1} - \frac{\tanh\frac{1-2z}{2\epsilon}}{\left(C_0^2-1\right)\tanh\frac{1-2z}{2\epsilon}+C_0^2+1}\right), \quad (67)$$

$$\theta^c(z) \approx -\frac{\pi}{2} + 2\arctan\frac{C_0\,\mathrm{e}^{\frac{1+2z}{2\epsilon}}-1}{C_0\,\mathrm{e}^{\frac{1+2z}{2\epsilon}}+1} + 2\arctan\frac{C_0\,\mathrm{e}^{\frac{1-2z}{2\epsilon}}-1}{C_0\,\mathrm{e}^{\frac{1-2z}{2\epsilon}}+1} - \epsilon\frac{2C_0\bar{\eta}\,\mathrm{e}^{\frac{1+2z}{2\epsilon}}}{\left(C_0^2\,\mathrm{e}^{\frac{1+2z}{\epsilon}}+1\right)^2} + \epsilon\frac{C_1\,\mathrm{e}^{\frac{1+2z}{2\epsilon}}}{C_0^2\,\mathrm{e}^{\frac{1+2z}{\epsilon}}+1} - \epsilon\frac{2C_0\bar{\eta}\,\mathrm{e}^{\frac{1-2z}{2\epsilon}}}{\left(C_0^2\,\mathrm{e}^{\frac{1-2z}{\epsilon}}+1\right)^2} + \epsilon\frac{C_1\,\mathrm{e}^{\frac{1-2z}{2\epsilon}}}{C_0^2\,\mathrm{e}^{\frac{1-2z}{\epsilon}}+1}. \quad (68)$$

The coefficients C_0 and C_1 can be determined by imposing the weak anchoring condition. Nevertheless, these latter depend on the particular value of $\gamma \geqslant 1$. Here, we focus on the cases $\gamma = 1$ and $\gamma = 2$. In the first case, by substituting the expansion (55) into the boundary conditions $(54)_I$ one obtains by working at $O(\epsilon)$

$$2\widetilde{\theta}_{0z}^- - \bar{\beta}\sin 2\widetilde{\theta}_0^- = 0; \quad (69)$$

$$\widetilde{\theta}_{1z}^- - \bar{\beta}\widetilde{\theta}_1^-\cos 2\widetilde{\theta}_0^- = 0. \quad (70)$$

By inserting equation (58) (with $A_1 = 1$) in (69), we arrive at

$$C_0 = \sqrt{\frac{\bar{\beta}+1}{\bar{\beta}-1}}. \quad (71)$$

Note that, $\bar{\beta}$ must be greater than 1. Indeed, by (19) (with $\alpha = 0$) the existence of non-trivial solutions requires $\beta \geqslant V_S\tanh(V_S/2)$; furthermore the reduced applied potential V must be less than V_S and, consequently, $\beta \geqslant V_S\tanh(V_S/2) > V\tanh(V/2)$. Now, since $\beta = \bar{\beta}/\epsilon$ and $V = 1/\epsilon$, for an infinitesimal ϵ it follows that $\bar{\beta} > 1$.

If we replace (58) and (64) into (70) we arrive at

$$C_1 = \sqrt{\frac{\bar{\beta}+1}{\bar{\beta}-1}}\bar{\eta}. \quad (72)$$

In the case $\gamma = 2, \widetilde{\theta}_0^-$ is fixed to be zero, which implies $C_0 = 1$. Consequently, after some algebra, equation (58) becomes identical to (4.20) in [14]. Thus, at $O(1)$, and if β increases sufficiently rapidly with ϵ, the solution does not distinguish between weak and strong anchoring. Nevertheless, some difference occurs at the successive orders. In particular

when $\gamma = 2$, we obtain

$$C_1 = \bar{\eta} + \frac{2}{\bar{\beta}}, \tag{73}$$

which depends on the anchoring strength. Note that, with respect to the previous case, now $\bar{\beta}$ may assume any positive values.

4.4. Small nematic anisotropies

In the previous subsections, our results have been derived in the case of vanishing nematic anisotropy, $\alpha = 0$. To make a direct comparison with the results of the literature we need to extend our results to the case of small nematic anisotropies $\alpha = \epsilon\bar{\alpha}$, where $\bar{\alpha}$ is $O(1)$. For shortness, we here report only the expression of the composite solutions.

The solution ψ^c is still of the form (67). This means that ψ^c is not affected by the presence of a small nematic anisotropy. Indeed, the composite solution ψ^c depends on the anchoring strength through the constant C_0 which is given by (71) in the case $\gamma = 1$ or $C_0 = 1$ if $\gamma > 1$. However, in the case of perfect strong anchoring, $C_0 = 1$ and equation (67) reduces to the formula (4.26) of [14], provided by redefining z as $z + 1/2$.

The composite solution $\theta^c_{\bar{\alpha}}$ becomes

$$\theta^c_{\bar{\alpha}} = \theta^c + \vartheta^c, \tag{74}$$

where θ^c is given by (66) and

$$\vartheta^c \approx -\epsilon \frac{C_0\, \mathrm{e}^{\frac{1+2z}{2\epsilon}}\big(C_0^2\, \mathrm{e}^{\frac{1+2z}{\epsilon}}\big(1+\frac{1+2z}{\epsilon}\big)+\frac{1+2z}{\epsilon}+5\big)\bar{\alpha}}{2\big(C_0^2\, \mathrm{e}^{\frac{1+2z}{\epsilon}}+1\big)^2} - \epsilon \frac{C_0\, \mathrm{e}^{\frac{1-2z}{2\epsilon}}\big(C_0^2 \mathrm{e}^{\frac{1-2z}{\epsilon}}\big(1+\frac{1-2z}{\epsilon}\big)+\frac{1-2z}{\epsilon}+5\big)\bar{\alpha}}{2\big(C_0^2 \mathrm{e}^{\frac{1-2z}{\epsilon}}+1\big)^2}. \tag{75}$$

The coefficient C_1 of the $\theta^c_{\bar{\alpha}}$ expression becomes

$$C_1 = \frac{4 - 3\bar{\beta} - 2\bar{\beta}^2 + 3\bar{\beta}^3}{2\bar{\beta}(1+\bar{\beta})(\bar{\beta}-1)^{3/2}}\bar{\alpha} + \sqrt{\frac{\bar{\beta}+1}{\bar{\beta}-1}}\bar{\eta} \qquad \text{if} \quad \gamma = 1, \tag{76}$$

$$C_1 = \frac{3}{2}\bar{\alpha} + \bar{\eta} + \frac{2}{\bar{\beta}} \qquad \text{if} \quad \gamma = 2. \tag{77}$$

In the case of strong anchoring we have $C_1 = 3\bar{\alpha}/2 + \bar{\eta}$. After some tedious but straightforward algebra we recover equation (4.27) of [14], providing to change z in $z + 1/2$.

4.5. Discussion

The analysis in the strong electric field regime has been performed by taking into account just small dielectric anisotropies and one constant approximation (or small nematic anisotropy). In fact, our study has been intentionally addressed to point out some differences that arise if we introduce a finite anchoring energy rather than an infinite one. Thus, we have retained the minimum number of parameters in order to simplify our discussion. However, the study could be extended to several regimes of dielectric and nematic anisotropies pursuing similar developments adopted in section 4.3 of [14]. Nevertheless, the study for small anisotropy regimes could have an experimental counterpart for certain types of nematic liquid crystals (see, for example, [11]). In addition, large nematic anisotropies may give rise to out of plane distortions.

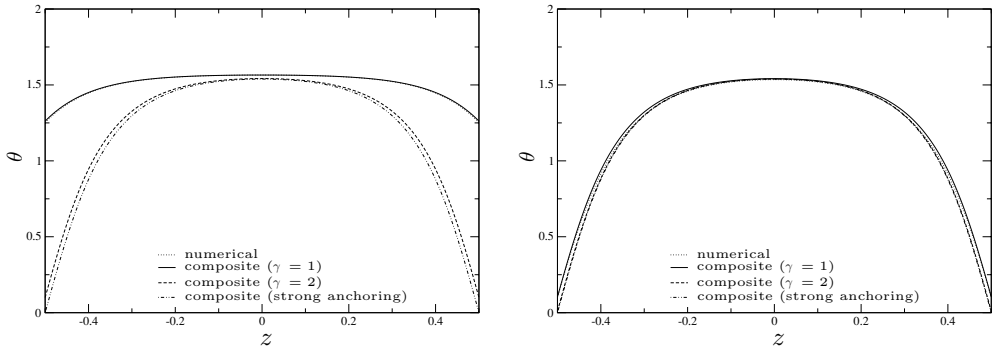

Figure 5. Plots of numerical and composite solutions with $V = 3\pi$, $\beta = 10$ (left) and $\beta = 100$ (right). Both plots have been obtained in one constant approximation hypothesis and dielectric anisotropy $\eta = 0.2$.

Note that γ is not an artificial parameter introduced to make the scaling work. Indeed, since $\bar{\beta}$ is $O(1)$ we can deduce $\gamma \simeq \ln\beta/\ln V$. The so-obtained γ is related to the order beyond which the anchoring effects manifest themselves in the approximate equilibrium solution. If $\gamma = 1$ then the weak anchoring takes place at $O(1)$ approximation. If $\gamma \geqslant 2$, weak and strong anchoring solutions coincide up to $O(\epsilon^{\gamma-2})$ and the weak anchoring effects occur beyond $O(\epsilon^{\gamma-2})$. Figure 5 shows the plots of θ through the sample, given by numerical simulation and the composite solutions. In the left plot the numerical simulation is obtained by setting $\beta = 10$ and $V = 3\pi$, and since these two parameters are both sufficiently larger than 1, we can appreciate the boundary layers. The ratio between β and V yields an estimate of the γ value. In this case, since β and V are of the same order of magnitude, we may refer to $\gamma \simeq 1$. Thus, the composite solution with $\gamma = 1$ is practically indistinguishable from the numerical one, as is well proved by figure 5. By contrast, analytical solution with much larger γ is quite different from the corresponding numerical solution. For example, if we consider $\beta = 100$ and $V = 3\pi$ (right plot of figure 5) then $\gamma \simeq 2$ is expected. In this case the $\gamma = 1$ composite solution is still indistinguishable from the numerical one. In addition, the $\gamma = 2$ composite solution is very close to the numerical solution and both are very similar to the solution with strong anchoring boundary conditions.

It is possible to show, by performing the derivative of (68), that the electric field inside the cell shows a quite similar behaviour to the θ profile: the boundary layers are more or less important depending on the anchoring strength.

We also remark that within the magnetic approximation limit, $\bar{\eta} = 0$. Thus, as expected, by (68) it follows $\psi^c = z$. The density of charge on the boundary is not affected by the distortion and, coherently, it is not affected by the anchoring energy.

Finally note that, in the regime of high applied fields the perfectly strong anchoring is obtained in the $\beta/V \to \infty$ limit.

5. Different anchoring strengths

In this section, we briefly discuss some effects that are derived by considering two different anchoring energies at the boundaries. In practice, this condition can be accomplished, for example, by applying a different type of surfactant for each delimiting surface.

At each plate, the easy axis is planar. If we use the results derived in section 2, we can first analyse the influence of the two different anchoring strengths on the critical thresholds

and study the solution for applied fields reaching the critical values. Then, we point out the results that concern high applied voltages.

5.1. Critical fields

The field (17) are still solutions of the equilibrium equations. We can apply the usual perturbation algorithm to calculate the critical fields and the form of the solutions close to them. We expand θ as in (21) and we replace (21) in (14)–(16). At $O(\delta)$ we obtain the linearized dimensionless bulk equilibrium equations (23) with the boundary conditions

$$\theta_{1z}^{\pm} \pm \beta^{\pm}\theta_1^{\pm} = 0, \qquad \psi_1^{\pm} = 0, \tag{78}$$

which admit the non-trivial solution

$$\theta_1 = A_1 \cos(V_F z) + A_2 \sin(V_F z). \tag{79}$$

$$\psi_1 = 0, \tag{80}$$

where V_F satisfies the equation

$$\left(V_F^2 - \beta^-\beta^+\right) \sin V_F - V_F(\beta^- + \beta^+) \cos V_F = 0. \tag{81}$$

The constants A_1 and A_2 are now different in the general case. Therefore, due to the difference between the anchoring strengths, the solutions lose their symmetry with respect to $z = 0$. By imposing the boundary conditions on the linearized equations one can express, for example, A_1 as a function of A_2. Nevertheless, as in section 3, the solution remains undetermined at the first order; the determination of A_2 involves the order $O(\delta^3)$.

To study the threshold behaviour, we introduce β_M and $\Delta\beta$ defined as

$$\beta_M = \frac{\beta^+ + \beta^-}{2}, \qquad \Delta\beta = \frac{\beta^+ - \beta^-}{2}. \tag{82}$$

Then, equation (81) becomes

$$\left[V_F^2 - {\beta_M}^2 + (\Delta\beta)^2\right] \sin V_F - 2\beta_M V_F \cos V_F = 0. \tag{83}$$

Without loss of generality, we may assume $\beta^- \leqslant \beta^+$. It follows that $0 \leqslant \Delta\beta \leqslant \beta_M$, since both dimensionless anchoring strengths are positive. Then, $\Delta\beta = 0$ corresponds to the case treated in previous sections, while $\Delta\beta = \beta_M$ corresponds to the situation with free boundary conditions at $z = -1/2$.

For all positive, fixed β_M, $V_F(\Delta\beta)$ defined by (82) is a decreasing monotonic function in $[0, \beta_M]$ (see figure 4, left). The maximum value is given by equation (18), while the minimum value satisfies

$$\frac{V_F}{\beta^+} = \cot V_F, \tag{84}$$

which occurs when free orientations of the director at one of the plates are considered.

In a similar way, we can determine the saturation threshold. By expanding θ as in (37) and working at $O(\delta)$ we obtain the linear solutions

$$\bar{\theta}_1 = \bar{A}_1 \cosh \frac{V_S z}{\sqrt{\iota}} + \bar{A}_2 \sinh \frac{V_S z}{\sqrt{\iota}}, \tag{85}$$

where the critical threshold V_S obeys the following equation:

$$\left[\iota V_S^2 + \beta_M^2 - (\Delta\beta)^2\right] \sinh \frac{V_S}{\sqrt{\iota}} - 2\beta_M \sqrt{\iota} V_S \cosh \frac{V_S}{\sqrt{\iota}} = 0. \tag{86}$$

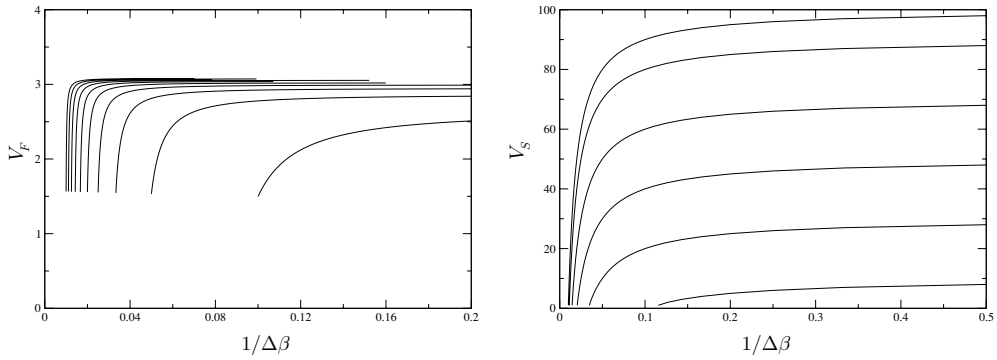

Figure 6. Plots of the Freedericksz threshold V_F (left) and saturation threshold V_S (right) as a function of the inverse of the anchoring strength difference $\Delta\beta$ for various values of β_M. In both plots the curves move upwards as the value of β_M increases.

Just as V_F, for all positive, fixed β_M, $V_S(\Delta\beta)$ is a decreasing monotonic function in $[0, \beta_M]$ (see figure 6, right). The maximum value satisfies equation (19), while the minimum value obeys

$$\frac{V_S}{\beta^+} = \frac{1}{\sqrt{\iota}} \coth \frac{V_S}{\sqrt{\iota}}. \tag{87}$$

Plots of V_F (left) and V_S (right) as a function of the inverse of the anchoring strength difference $\Delta\beta$ for different values of β_M are shown in figure 6. In both plots the curves move upwards as the mean anchoring strength increases. In the plots of V_F, in each curve the minimum satisfies equation (84). In the $\beta \to \infty$ limit, the curve of V_F consists of two linear parts: a first one, almost vertical, between $\pi/2$ and π, grazing the $\Delta\beta = 0$ axis, and a second horizontal one, which approaches $V_F = \pi$. In particular, if $1/\Delta\beta$ is infinitesimal, the critical value tends to $\pi/2$, which is the Freedericksz threshold of a sample with strong planar anchoring boundary conditions on one plate and freely orientable molecules on the other one. By contrast, if $\Delta\beta$ is infinitesimal we recover the classical Freedericksz threshold $V_F = \pi$.

On the other hand, V_S exhibits radically different properties with respect to V_F. In the $\beta_M \to \infty$ limit the solution of (87) gives $V_S \to \infty$. This means that, it is sufficient to have just strong anchoring condition on one plate, to avoid the saturation transition. Nevertheless, we could have reached the same conclusion by observing that the trivial solution $(17)_2$ cannot hold when either β^+ or β^- goes to infinity.

In both plots, the maximum of each curve is reached at $\Delta\beta = \beta_M$, which corresponds to the case with the same anchoring energy at both plates. In agreement with equations (18) and (19), the critical fields are increasing functions of the anchoring strength.

5.2. High applied voltages

We finally analyse the case of small dielectric anisotropies and one constant approximation with a high applied voltage. With respect to the case treated in section 4, a loss of symmetry is expected in the composite solution. To obtain the composite solutions we can again apply similar arguments pursued in section 4. We set $V = 1/\epsilon$ and consider $\epsilon \to 0$; we define $\bar{\beta}^{\pm} = \beta^{\pm}/\epsilon^{\gamma}$. The bulk equilibrium equations (46) and (47) and the boundary conditions (54) do not change, while the boundary conditions (54) become

$$2\epsilon^{\gamma-1}\widetilde{\theta}^-_{\zeta} \pm \bar{\beta}^{\pm} \sin 2\widetilde{\theta}^- = 0. \tag{88}$$

Thus, the results obtained in section 4 can be adapted to make the constants of the solution compatible with the boundary condition (88). For shortness, we just focus on some relevant results. When the asymptotic matching is completed, the solutions of both left and right inner problems become

$$\widetilde{\psi}^l \approx -\frac{1}{2} + \epsilon\zeta + \epsilon^2 \frac{4\bar{\eta} C_{l_0}^2 \tanh\zeta}{\left(C_{l_0}^2+1\right)\left[\left(C_{l_0}^2-1\right)\tanh\zeta + C_{l_0}^2+1\right]}, \tag{89}$$

$$\widetilde{\theta}^l \approx 2\arctan\frac{C_{l_0}\,\mathrm{e}^{\zeta}-1}{C_{l_0}\,\mathrm{e}^{\zeta}+1} - \epsilon\frac{2C_{l_0}\bar{\eta}\,\mathrm{e}^{\zeta}}{\left(C_{l_0}^2\mathrm{e}^{2\zeta}+1\right)^2} + \epsilon\frac{C_{l_1}\mathrm{e}^{\zeta}}{C_{l_0}^2\,\mathrm{e}^{2\zeta}+1}, \tag{90}$$

$$\widetilde{\psi}^r \approx \frac{1}{2} - \epsilon\zeta - \epsilon^2 \frac{4\bar{\eta} C_{r_0}^2 \tanh\zeta}{\left(C_{r_0}^2+1\right)\left[\left(C_{r_0}^2-1\right)\tanh\zeta + C_{r_0}^2+1\right]}, \tag{91}$$

$$\widetilde{\theta}^r \approx 2\arctan\frac{C_{r_0}\,\mathrm{e}^{\zeta}-1}{C_{r_0}\,\mathrm{e}^{\zeta}+1} - \epsilon\frac{2C_{r_0}\bar{\eta}\,\mathrm{e}^{\zeta}}{\left(C_{r_0}^2\mathrm{e}^{2\zeta}+1\right)^2} + \epsilon\frac{C_{r_1}\mathrm{e}^{\zeta}}{C_{r_0}^2\,\mathrm{e}^{2\zeta}+1}, \tag{92}$$

where the constants with subscript l depend on β^- and those with subscript r depend on β^+. The outer solution reads

$$\widehat{\psi} \approx z + \frac{\epsilon^2(1-2z)}{C_{l_0}^2+1} - \frac{\epsilon^2(1+2z)}{C_{r_0}^2+1}, \qquad \widehat{\theta} \approx \frac{\pi}{2}. \tag{93}$$

Consequently, the composite solutions are

$$\begin{aligned}\psi^c(z) \approx z - \frac{\epsilon^2(1-2z)}{C_{l_0}^2+1} + \frac{\epsilon^2(1+2z)}{C_{r_0}^2+1} + \Bigg(&\frac{\tanh\frac{1+2z}{2\epsilon}}{\left(C_{l_0}^2-1\right)\tanh\frac{1+2z}{2\epsilon}+C_{l_0}^2+1} \\ &- \frac{\tanh\frac{1-2z}{2\epsilon}}{\left(C_{r_0}^2-1\right)\tanh\frac{1-2z}{2\epsilon}+C_{r_0}^2+1}\Bigg),\end{aligned} \tag{94}$$

$$\begin{aligned}\theta^c(z) \approx -\frac{\pi}{2} &+ 2\arctan\frac{C_{l_0}\,\mathrm{e}^{\frac{1+2z}{2\epsilon}}-1}{C_{l_0}\,\mathrm{e}^{\frac{1+2z}{2\epsilon}}+1} + 2\arctan\frac{C_{r_0}\,\mathrm{e}^{\frac{1-2z}{2\epsilon}}-1}{C_{r_0}\,\mathrm{e}^{\frac{1-2z}{2\epsilon}}+1} \\ &- \epsilon\frac{2C_{l_0}\bar{\eta}\mathrm{e}^{\frac{1+2z}{2\epsilon}}}{\left(C_{l_0}^2\,\mathrm{e}^{\frac{1+2z}{\epsilon}}+1\right)^2} + \epsilon\frac{C_{l_1}\,\mathrm{e}^{\frac{1+2z}{2\epsilon}}}{C_{l_0}^2\,\mathrm{e}^{\frac{1+2z}{\epsilon}}+1} - \epsilon\frac{2C_{r_0}\bar{\eta}\,\mathrm{e}^{\frac{1-2z}{2\epsilon}}}{\left(C_{r_0}^2\,\mathrm{e}^{\frac{1-2z}{\epsilon}}+1\right)^2} + \epsilon\frac{C_{r_1}\,\mathrm{e}^{\frac{1-2z}{2\epsilon}}}{C_{r_0}^2\,\mathrm{e}^{\frac{1-2z}{\epsilon}}+1}.\end{aligned} \tag{95}$$

The undetermined constants can be deduced by requiring that the weak boundary condition is satisfied. If the reduced anchoring strengths scale with $\gamma = 1$ we obtain

$$C_{l_0} = \sqrt{\frac{\bar{\beta}^- + 1}{\bar{\beta}^- 1}}, \qquad C_{r_0} = \sqrt{\frac{\bar{\beta}^+ + 1}{\bar{\beta}^+ - 1}}, \tag{96}$$

$$C_{l_1} = \sqrt{\frac{\bar{\beta}^- + 1}{\bar{\beta}^- 1}}\bar{\eta}, \qquad C_{r_1} = \sqrt{\frac{\bar{\beta}^+ + 1}{\bar{\beta}^+ - 1}}\bar{\eta}. \tag{97}$$

If $\beta^- = \beta^+ = \beta$, it is easy to verify that $C_{l_0} = C_{r_0}$ and $C_{l_1} = C_{r_1}$. Then, the composite solutions (94) and (95) take the form (67) and (68), respectively. We also remark that if $\gamma > 1$, we have that θ^c is an even function at $O(1)$; the loss of symmetry occurs at higher orders.

6. Concluding remarks

We have analysed plane deformations induced by an electrostatic field on a simple nematic cell, when finite anchoring energies at the boundaries are taken into account. We have deduced the approximate solutions close to the transition thresholds, through a regular perturbation method. We have also investigated the regime of high electric field obtaining solutions of boundary layer type. The effects of two different anchoring energies at the plates on the critical fields and on the form of solutions have also been analysed.

All analytical approximate results agree with the numerical solutions of the complete nonlinear problem. Also, within the strong anchoring limit we recover some known results [12, 14].

Future developments can be pursued in several ways. Certain type of nematic liquid crystals, such as PAA or MBBA, exhibit negative dielectric anisotropies. Therefore, their molecules tend to avoid the alignment with the electric field. One may analyse the plane distortions induced by an electric field on a simple cell of nematic liquid crystals with negative dielectric anisotropy and weak anchoring at the boundary which favour homeotropic boundary conditions.

However, a more exhaustive study should take into account the extension to spatial deformations. This extension will involve further terms in the energy functional: the twist energy in the bulk and the saddle-splay energy on the boundary [17]. Furthermore, one may also take into account different forms of anchoring energy with respect to the Rapini–Papoular formula.

Further developments could be done within the Landau–de Gennes theory. In this direction, the mutual interaction between the electric field and the order tensor Q for a simple cell of nematic with strong planar boundary conditions is taken into account in [18]. Interesting results concerning the weak anchoring for confined nematics subjected to magnetic fields are reported in [19, 20].

Acknowledgments

I wish to thank Paolo Biscari for his critical comments and suggestions. This work was made possible by the Post-Doctoral Fellowship ‘Mathematical Models for Fluid Membranes’, supported by the Mathematical Department of the *Politecnico di Milano*.

References

[1] de Gennes P G and Prost J 1993 *The Physics of Liquid Crystals* 2nd edn (Oxford: Clarendon)
[2] Oseen C W 1933 The theory of liquid crystals *Trans. Faraday Soc.* **29** 883
[3] Zocher H 1933 The effect of a magnetic field on the nematic state *Trans. Faraday Soc.* **29** 945
[4] Frank F C 1958 On the theory of liquid crystals *Disc. Faraday Soc.* **25** 19
[5] Virga E G 1994 *Variational Theories for Liquid Crystals* (London: Chapman and Hall)
[6] Brian-Brown G P, Wood E L and Sage I C 1999 Weak surface anchoring of liquid crystals *Nature* **399** 338
[7] Rapini A and Papoular M 1969 Distortion d’une lamelle nématique sous champ magnétique. Conditions d’angrage aux paroix *J. Phys. Coll.* **30** 54
[8] Naemura S 1978 Measurement of anisotropic interfacial interaction between a nematic liquid crystal and various substrates *Appl. Phys. Lett.* **33** 1
[9] Freedericksz V and Zolina V 1933 Forces causing the orientation of an anisotropic liquid *Trans. Faraday Soc.* **29** 919
[10] Deuling H 1972 Deformation of nematic liquid crystals in an electric field *Mol. Cryst. Liq. Cryst.* **19** 123
[11] Gruler H and Meier G 1972 Electric field-induced deformations in oriented liquid crystals of the nematic type *Mol. Cryst. Liq. Cryst.* **16** 299

[12] Schiller P 1989 Perturbation theory for planar nematic twisted layers *Liq. Cryst.* **4** 69
[13] Blake G I, Mullin T and Tavener S J 1999 The Freedericksz transition as a bifurcation problem *Dyn. Stab. Syst.* **14** 299
[14] Self R H, Please C P and Sluckin T J 2002 Deformation of nematic liquid crystals in an electric field *Euro. J. Appl. Math.* **13** 1
[15] Strigazzi A 1988 Surface elasticity and Freedericksz threshold in a nematic cell weakly anchored *Nuovo Cimento* D **10** 1335
[16] Hinch E J 1991 *Perturbation Methods* (Cambridge: Cambridge University Press)
[17] Kiselev A D 2004 Saddle-splay-term-induced orientational instability in nematic-liquid-crystal cells and director fluctuations at substrates *Phys. Rev.* E **69** 041701
[18] Cesana P 2005 Effetti di disordine termico sulle interazioni tra cristalli liquidi nematici e campi elettrici e magnetici *Tesi di Laurea* Politecnico di Milano, Milano
[19] Mottram N J and Hogan S J 2002 Magnetic field-induced changes in molecular order in nematic liquid crystals *Contin. Mech. Thermodyn.* **14** 281
[20] Sarlah A 2001 Effect of the confining substrates on nematic order-fluctuations in liquid crystals *PhD Thesis* University of Ljubljana